AIP | Review of Scientific Instruments

Design and operation of the wide angular-range chopper spectrometer ARCS at the Spallation Neutron Source

D. L. Abernathy, M. B. Stone, M. J. Loguillo, M. S. Lucas, O. Delaire et al.

Citation: Rev. Sci. Instrum. **83**, 015114 (2012); doi: 10.1063/1.3680104
View online: http://dx.doi.org/10.1063/1.3680104
View Table of Contents: http://rsi.aip.org/resource/1/RSINAK/v83/i1
Published by the American Institute of Physics.

Design and operation of the wide angular-range chopper spectrometer ARCS at the Spallation Neutron Source

D. L. Abernathy,[1,a)] M. B. Stone,[1] M. J. Loguillo,[1] M. S. Lucas,[1,b)] O. Delaire,[1]
X. Tang,[2] J. Y. Y. Lin,[2] and B. Fultz[2]
[1]*Neutron Scattering Sciences Division, Oak Ridge National Laboratory, 1 Bethel Valley Road, Oak Ridge, Tennessee 37831, USA*
[2]*California Institute of Technology, W. M. Keck Laboratory 138-78, Pasadena, California 91125, USA*

(Received 14 July 2011; accepted 4 January 2012; published online 31 January 2012)

The wide angular-range chopper spectrometer ARCS at the Spallation Neutron Source (SNS) is optimized to provide a high neutron flux at the sample position with a large solid angle of detector coverage. The instrument incorporates modern neutron instrumentation, such as an elliptically focused neutron guide, high speed magnetic bearing choppers, and a massive array of ^{3}He linear position sensitive detectors. Novel features of the spectrometer include the use of a large gate valve between the sample and detector vacuum chambers and the placement of the detectors within the vacuum, both of which provide a window-free final flight path to minimize background scattering while allowing rapid changing of the sample and sample environment equipment. ARCS views the SNS decoupled ambient temperature water moderator, using neutrons with incident energy typically in the range from 15 to 1500 meV. This range, coupled with the large detector coverage, allows a wide variety of studies of excitations in condensed matter, such as lattice dynamics and magnetism, in both powder and single-crystal samples. Comparisons of early results to both analytical and Monte Carlo simulation of the instrument performance demonstrate that the instrument is operating as expected and its neutronic performance is understood. ARCS is currently in the SNS user program and continues to improve its scientific productivity by incorporating new instrumentation to increase the range of science covered and improve its effectiveness in data collection. © *2012 American Institute of Physics*. [doi:10.1063/1.3680104]

I. INTRODUCTION

ARCS is a wide angular-range, direct-geometry, time-of-flight chopper spectrometer at the Spallation Neutron Source (SNS), Oak Ridge National Laboratory (ORNL). This class of inelastic neutron scattering instruments is characterized by the use of a Fermi chopper[1] consisting of stacked, thin neutron-absorbing slats rotating at high speed in the flight path from the pulsed source to the sample.[2] By delaying the opening of the path through the Fermi chopper relative to the neutron generation by a known time, a short burst of monochromatic neutrons is incident on the sample. Detectors positioned around the sample are used to calculate the final neutron energy from the total time-of-flight, thus providing the energy transfer $\hbar\omega$, and with the scattering angle of the detected neutrons, the momentum transfer $\boldsymbol{Q}$ is determined. Chopper spectrometers at spallation neutron sources over three decades have successfully measured dynamics in condensed matter systems from a few meV to hundreds of meV covering a broad range of scientific areas. For example, early studies included atomic vibrations in crystals[3] and amorphous solids,[4] and crystal field transitions.[5] As instrumentation has advanced, more challenging experiments, for example to determine the momentum distributions in quantum liquids[6] and spin dynamics in low-dimensional magnetic systems,[7] have become possible. Thus during preliminary discussions of the instrument suite at the SNS, high incident energy chopper spectrometers were included as essential tools to study excitations in materials,[8] and ARCS is the final result from one of those spectrometer concepts.

The design of ARCS owes much to previous chopper spectrometers at pulsed neutron sources. It is intentionally based on proven concepts, as it is one of the first instruments to operate at the SNS and should be productive immediately. Instruments such as HRMECS and LRMECS at the Intense Pulsed Neutron Source, Argonne National Laboratory (US),[9] INC at the KEK Neutron Science Laboratory (Japan),[10] and HET and MARI at the ISIS facility, Rutherford Appleton Laboratory (UK) (Ref. 11) have all provided important lessons. The use of highly pixelated detector arrays was employed successfully by PHAROS at the Lujan Center, Los Alamos National Laboratory (US) (Ref. 12) and MAPS at ISIS.[13] Optimization for single crystal studies was a particular emphasis of the MAPS developments, which also demonstrated the critical importance of software for data visualization and analysis for advanced chopper spectrometers.[14] ARCS is among a new generation of chopper spectrometers that builds on the heritage of previous instruments and includes advances in neutron instrumentation such as the use of neutron guides to enhance the flux on sample at lower incident energies. MERLIN at ISIS,[15] HRC and 4SEASONS at the Japanese Proton Accelerator Research Complex,[16] and SEQUOIA at the SNS (Ref. 17) are recently operational examples. The ARCS design emphasizes high-flux measurements over a

a)Author to whom correspondence should be addressed. Electronic mail: abernathydl@ornl.gov.
b)Current address: Air Force Research Laboratory, Wright-Patterson AFB, Ohio 45433, USA.

wide range of scattering angles with incident energies, E_i, from 15 meV up to several eV with an elastic energy resolutions of the order of 3% to 5% of E_i (full width at half maximum) in standard operating conditions.[18] The instrument has been optimized for the source characteristics and physical constraints of the SNS.[19]

ARCS is a member of a suite of seven inelastic instruments in operation or under construction at the SNS, each spectrometer providing differently optimized conditions for the resolution and range of both momentum transfer, $\boldsymbol{Q}$, and energy transfer, $\hbar\omega$.[20] Of the currently operating instruments, NSE (neutron spin echo),[21] BASIS (backscattering spectrometer),[22] and CNCS (direct geometry spectrometer)[23] all provide finer energy resolution than ARCS. SEQUOIA, the other Fermi chopper spectrometer, provides for somewhat finer resolution than ARCS with an emphasis on detector coverage in the forward direction to measure magnetic scattering. SEQUOIA is also supporting users as it finishes its commissioning phase.[24] Future spectrometers at the SNS include HYSPEC,[25] utilizing polarized beams, and a high throughput chemical spectroscopy instrument, VISION. ARCS also complements the existing triple-axis capabilities at the High Flux Isotope Reactor (HFIR) at ORNL by covering large volumes of $\boldsymbol{Q}$ and $\hbar\omega$ space efficiently.[26]

The project to construct ARCS was initiated in 2001 when an Instrument Development Team (IDT) consisting of researchers using inelastic neutron scattering was formed to propose a new instrument to be built at the SNS, which was still in early development itself. The US Department of Energy (DOE) provided a grant to the California Institute of Technology (Caltech) to fund the bulk of the purchases for the spectrometer, along with support for the design effort through Oak Ridge National Laboratory. Work on the hardware of the spectrometer started in earnest in 2002, and first neutrons were measured in 2007.

As an acknowledgement that software plays a key role in the scientific productivity of new neutron scattering facilities, funds were included in the Caltech grant to develop software for data reduction and analysis. The software development was carried out at Caltech with help from the SNS team, and monitored and critiqued by the IDT. The ARCS reduction software produced, known as DRCS or DrChops,[27] was one of the first packages that reduces event-mode neutron data, where the traditional histogramming approach is replaced by a system to record the pixel location and time of flight of each detected neutron, directly to spectra of physical interests such as S(Q) and S(Q,E). The software was instrumental in the commissioning of the ARCS instrument by providing both scripting and graphical tools that quickly reduce and analyze data, and help in diagnosing the instrument performance. With some updates, the original software is still in use today.

ARCS has been undergoing scientific commissioning and user operations since 2008 and has been fortunate enough to be scientifically productive almost immediately. The rise in interest in iron-based superconductors corresponded well to the ARCS scientific mission. The early experiments on ARCS led to significant results measuring phonon density-of-states (PDOS) (Ref. 28) and subsequent single crystal magnetism studies[29–31] of these materials. ARCS has also been used to study the PDOS of thermoelectric materials[32] and alloys,[33] and has been characterized as a diffractometer in anticipation of use for dynamic pair distribution function studies.[34] The ARCS instrument is in operations within the SNS user program and the ARCS IDT continues its involvement by allocating 20% of the user beam time to exciting science and development projects from among these core users.

In the remaining sections, a detailed description of the design and operation of ARCS is given, with an emphasis on novel features of the spectrometer. Initial measurements to determine the performance of ARCS are described and compared to analytical results and simulations. Examples of current scientific results are discussed along with future developments for the instrument.

II. DESIGN AND OPERATION OF ARCS

Figure 1 is a rendering of ARCS with the major instrument components labeled. A summary of key instrument parameters is given in Table I. Several optical components of ARCS reside within the SNS target monolith. The neutron source is a decoupled, ambient temperature water moderator with a poison depth of 25 mm. This provides the best flux of the SNS moderators in the thermal to epithermal range.[35] The core vessel insert is a defining aperture to limit the view of the subsequent beamline to the 10 cm × 12 cm (H × V) moderator face. The 30-ton beamline primary shutter carries a shutter insert with neutron guide. The shutter insert is aligned by kinematic mounts when open, providing a reproducible location for the 1.9 m long, $m = 2.5$ index supermirror guide. Within the monolith and along the incident beamline, a combination of poured heavy concrete, stacked steel, and formed heavy and regular concrete blocks provide the necessary biological and instrument background shielding.

One of the technical challenges addressed by the ARCS instrument is the design of a new T_0 neutron chopper, necessary to block the fast radiation from the source when the proton beam hits the target, i.e., at zero time-of-flight. The

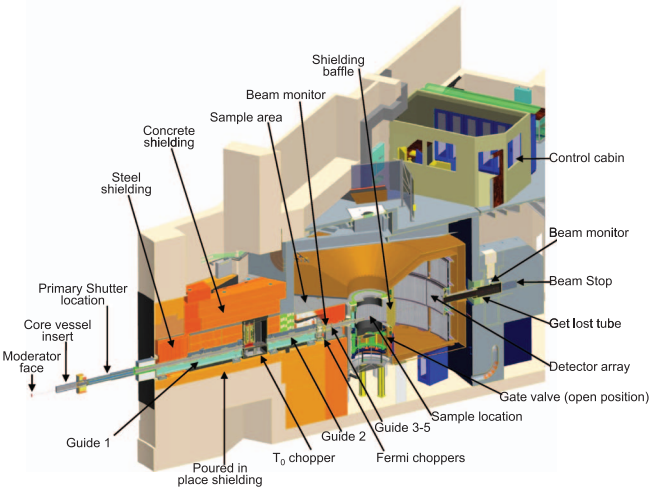

FIG. 1. (Color online) Overview rendering of ARCS with components labeled. Instrument components are described in the text and in Table I. The instrument's primary shutter is not illustrated and the first radial shielding baffle is not illustrated for clarity of the figure.

TABLE I. ARCS instrument parameters. Detector coverage and location of instrument components are further discussed in the text and shown in Fig. 1.

SNS beamline	18
Moderator	Decoupled ambient water poisoned at 25 mm
Incident energy range, E_i (meV)	15–1500 typical extends up to 5000
Energy resolution for elastic scattering	3.0% to 5.0% of E_i
Moderator to T_0 chopper distance (m)	8.77
Moderator to Fermi chopper distance (m)	11.61
Fermi chopper to sample distance (m)	1.99
Sample to detector distance (m)	3.0 to 3.5
Moderator to beam monitor 1 (m)	11.83
Moderator to beam monitor 2 (m)	18.50
Shutter guide length, $m = 2.5$ (m)	1.9
Elliptical guide length, $m = 3.6$ (m)	7.9
Maximum beam size at sample (mm)	50 × 50
Detectors	Position sensitive ^{3}He tubes at 10 atm
Detector tube dimensions	1 m long × 25.4 mm dia.
Detector configuration	Cylindrical
Number of tubes	920 = 8 × 115 packs
Pixels per tube	128
Detector coverage solid angle (sr) [overall range]	$2.5 = 0.8\pi$
Horizontal detector coverage (°)	−28 to 135
Vertical detector coverage (°)	−27 to 26
Minimum detector angle (°)	3
Volume of sample vacuum chamber (m^3)	10
Volume of detector vacuum chamber (m^3)	70

ARCS T_0 chopper not only blocks the prompt radiation from the source but also eliminates unwanted neutrons from the incident beam line by utilizing a vertical-axis design inspired by the "sloppy" choppers in the Intense Pulsed Neutron Source spectrometers. This design has been developed in collaboration with the SNS instruments SEQUOIA and HYSPEC, working with SKF Magnetic Bearings.[36] The T_0 chopper rotor consists of 175 kg of Inconel 718 alloy machined in a truncated elliptical shape with a neutron path ~8.5 cm wide by 8.5 cm tall bored along the major axis. Figure 2(a) shows a line drawing of the rotor and a photograph of two rotors. The shape has been optimized to reduce the rotating mass while preserving a roughly constant amount of material in the beam for different phase angles relative to the neutron flight path. Figure 2(b) is a photograph of the ARCS T_0 chopper assembly. The rotor is supported from above by a magnetic bearing system within a vacuum housing, with all connections made through an interface designed for remote handling. Because the system uses magnetic bearings, it is maintenance free and can spin up to 180 Hz, three times the 60 Hz SNS source frequency. The rotor has been carefully designed and tested as a "prime reliable" component, similar to the requirement for rotating jet engine parts, since the plane of rotation might allow debris to fly toward the source in the case of a catastrophic failure. The high speed means that the efficiency of blocking the prompt radiation is still at its maximum even when the chopper is phased to pass 1500 meV neutrons and provides some blocking up to 5 eV. Use of the T_0 chopper without

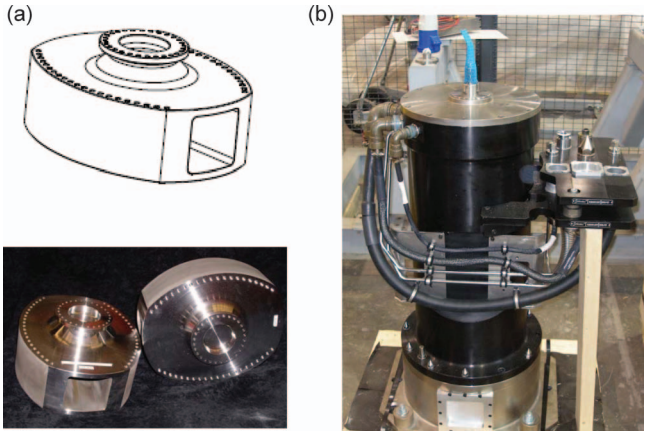

FIG. 2. (Color online) (a) Line drawing and pictures of T_0 chopper rotors. The 175 kg rotor is supported and rotated by a vertical-axis magnetic bearing system. (b) Photograph of the T_0 chopper system. The height of the full housing is 1.1 m.

a Fermi chopper in the beam has proven useful as a broad band-pass source for detector calibrations, sample alignment, and diffraction. ARCS was built to accommodate a second T_0 chopper adjacent to the first, providing a potential improvement of the signal-to-noise ratio for measurements, particularly in the eV range of incident energies.

Along the incident flight path from the shutter to the sample position, there are 7.9 m of high index ($m = 3.6$) elliptically shaped supermirror guide, which boosts the flux on the sample in the lower E_i range. The three regions of neutron guide with five sections are shown in Fig. 1. The guide was designed to provide flexibility for future adaptation to differing requirements for the beam divergence and size. A short piece of neutron guide after the Fermi chopper (guide section 3 seen in Fig. 3) is designed to be replaceable in the future with different incident optics, e.g., a single or crossed Soller collimator. A portion of the guide system (sections 4 and 5) extends into the scattering chamber, sharing its vacuum space. This eliminates a final aluminum guide window in the vicinity of the sample and reduces background. The last guide section just before the sample can be changed easily for different experiments, allowing the optics to be tailored for the different wavelengths and sample environments being used. This last guide section is also shown in Fig. 4, a photograph of the interior of the ARCS detector and sample vacuum spaces. A set of beam-defining motorized slits are currently in use in this area to adapt the beam size to the sample and sample environment.

For monochromating the neutron beam, ARCS has two Fermi choppers mounted on a translation stage 2.0 m upstream of the sample position (Fig. 3). These devices select the desired E_i by transmitting a short burst of neutrons at a defined time-of-flight relative to the source pulse. The magnetic bearing system supports a slit package consisting of alternating neutron absorbing slats and aluminum spacers, rotating at speeds up to 600 Hz and phase-locking to the source pulse to better than 1 μs. ARCS has four slit packages available, and a separate Fermi chopper system for mounting and testing of the chopper rotors before installation at the instrument. This

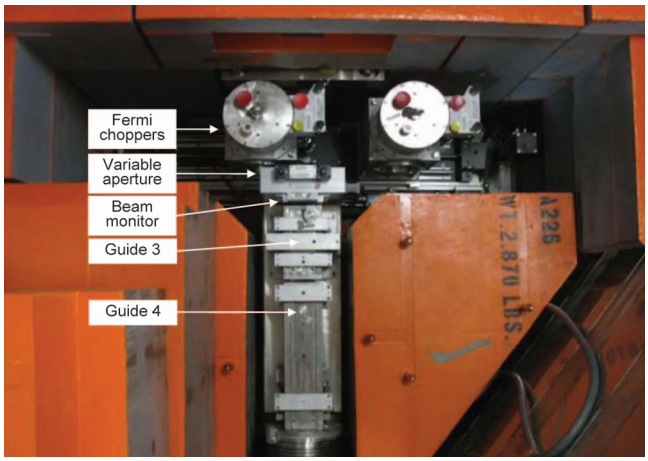

FIG. 3. (Color online) View from above of the neutron optics for ARCS just before the sample chamber. Neutrons travel from the guide system at the top, pass through one of two Fermi choppers mounted on a translation table, a variable aperture, beam monitor, and removable and fixed neutron guides. Guide 3 is a removable guide section. Guide 4 shares its vacuum with the sample chamber.

minimizes the downtime associated with adapting the choppers to the experimental requirements. The translation allows the two choppers to be swapped remotely within minutes, so that a broad range of excitations may be measured with optimized chopper settings for a given sample. This may be included in a script for automated data collection. There is a third position of this translation stage corresponding to having no Fermi chopper in the beam. The broad bands of wavelength that pass the vertical-axis T_0 chopper may be used, for example, to find the relative sensitivities of the detectors. By dephasing the T_0 chopper with respect to the neutron pulse, the full wavelength band of the source, a "white" beam, passes to the sample. Efficient powder diffraction data may be taken in this mode of sufficient quality to characterize sample ordering, for example.[34]

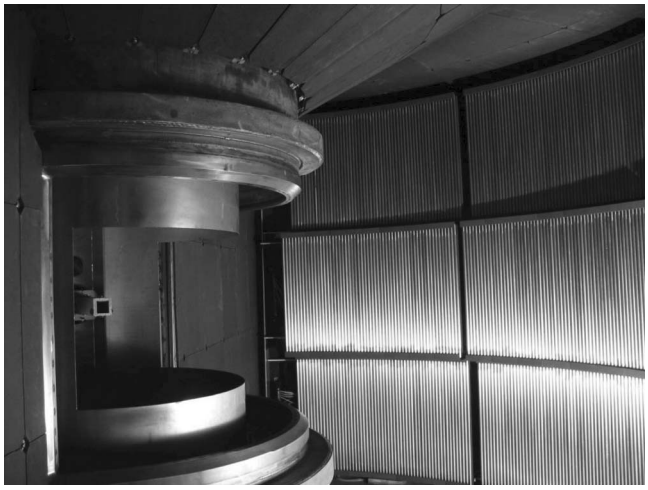

FIG. 4. View from the low angles toward the sample and high angle detectors. The neutron guide enters the sample chamber at the left, transporting neutrons to the sample position. A large semi-circular gate valve (shown in the open position) can be raised to isolate the sample volume for rapid changes of sample environment. The vertical gap in detector coverage shows the location of one of the scattered beam radial baffle positions which has subsequently been installed.

To take advantage of the flexibility of the ARCS chopper system, the ISAW software package[37] has been adapted to accept ARCS data and calculate Laue diffraction patterns for single crystal samples. Less than 1 min of data can provide a quick check of sample quality or phase and, depending on the sample, hundreds of peaks for single crystal lattice determination and orientation may be measured. The determined orientation may be saved as an orientation matrix or output in a format used by the single crystal inelastic scattering visualization software Mslice.[38] The use of existing diffraction software has improved the characterization of alignment of single crystals on ARCS considerably. One future development needed is to make the automatic refinement more tolerant of the larger mosaic samples and multicrystal arrays that are often used for inelastic scattering experiments.

After the Fermi chopper position there are several additional optical components in the ARCS main beampath. Figure 3 illustrates the locations of a motorized aperture with four independent blades, a beam monitor consisting of a low-pressure proportional ^{3}He gas detector, and two neutron guide sections. Two thin neutron absorbers on motorized actuators are also mounted here. Within the sample chamber, a second set of motorized blades may be mounted after neutron guide sections 4 or 5 to control the beam size immediately upstream of the sample position. After the beam has passed the sample, it exits the scattering chamber through a boron carbide lined beampath designed to reduce background from scattering of the beam after the sample and traverses a second low-efficiency beam monitor before being absorbed in the massive steel and heavy concrete beamstop.

Much of the novel design effort incorporated into ARCS is evident in the secondary spectrometer. To minimize background, it is necessary to eliminate as many windows as possible from the sample area to the neutron detectors. Doing this while maintaining fast experiment turn-around times and reliable detector operations was the technical challenge addressed. A primary example is the interface between the sample and detector vacuum spaces, shown in Figs. 1 and 4. A large, curved, vertically translating gate valve provides a means to isolate the two vacuum chambers for rapid changing of samples and sample environments without disturbing the much larger vacuum space of the detector vessel. In the down position, the gate valve provides a window-free final flight path from the sample to the detectors. After venting the sample chamber, a combination of a large mechanical pump with a Roots blower and a cryopump restores the vacuum to the 10^{-6} mbar range in under 15 minutes. At that time the gate valve may be opened without disturbing the vacuum of the detector chamber and neutron measurements may resume.

A cylindrical array of 115 modules or packs of eight 1-m long ^{3}He linear position sensitive detectors is installed within the detector vacuum chamber.[39] Figure 4 shows the view from the low angle area within the scattering chamber toward the neutron guide, sample position, and high angle detectors. To reduce background and increase safety by avoiding large, thin windows and to optimize space utilization, the detectors together with their digitizing electronics operate inside the

scattering chamber vacuum. The in-vacuum electronics also allows for a greater range of linear response of neutron counting rates for the neutron detectors by reducing the detector lead lengths before the preamplification stage to reduce noise. The heating of the electronics in vacuum is controlled by careful design using low power components, and the use of blackened surfaces on the electronics covers and facing detector chamber walls to enhance radiative thermal transfer from the packs. Further information regarding the detector configuration is described in Table I.

Because ARCS operates at high neutron energies, borated neutron shielding material was chosen for use in the vicinity of the incident and scattered neutron beams. A novel boron carbide based internal shielding material that uses no hydrogen in the binder material was developed,[40] known as zero hydrogen in product shielding (ZHIP mix). This material reduces the instrument's background signal and maintains vacuum performance of the vacuum chambers compared to the standard hydrogenous epoxy based shielding ("crispy" mix). Some of this material is shown in Fig. 4 lining the top and sides of the detector vacuum chamber. Additional shielding has subsequently been installed in both the sample and detector chambers, including radial absorbing baffles in the detector chamber. These reduce the background due to detector tube to detector tube scattering events.

ARCS uses the SNS data acquisition system, based on a central control computer managing satellite computers for different subsystems, such as motor control, sample environment, beam monitors, and the detector array controls. Data from the detector array are stored as a stream of neutron events, identifying the detector pixel and a time-of-flight value when the neutron was detected. The neutron events are correlated to the specific proton pulse which generated the neutrons from the source, and the pulse timestamp and proton charge are stored. Event-based data collection retains the maximum amount of information from the experiment and allows users to adjust or filter data sets based upon values of independent variables while histogramming the events in software. Gaps in the data which may occur for histogramming data acquisition systems due to limited memory and communication speed are eliminated. This improves the efficiency of measurement and more importantly enhances the flexibility of analysis after the experiment is finished. For example, continuous measurement while applying pump-probe techniques to a sample in the neutron beam, e.g., pulsed magnetic field application[41] or laser excitation, may be analyzed with different time binning after the experiment to optimize the statistics of the results relative to the rate of change of the signal measured.

ARCS has used this event based method to measure excitations in single crystals. Typically, a volume of reciprocal and energy space is measured by rotating the crystal about a vertical axis to predetermined positions, acquiring data at each location sequentially. Recording the motor position as a function of time while continuously rotating the sample allows the user maximum flexibility in determining the appropriate rotation bins, instead of requiring a fixed step size to be determined before the experiment begins. The entire measurement can be monitored so that the user determines when statistics are good enough for the desired signal or if the scan range can be reduced for more efficient data collection. This "sweep mode" of data collection is more tolerant of unforeseen features of the data and can increase measurement efficiency.

Historically the importance of software development in the full utilization of new neutron scattering instrumentation has been underappreciated. Fortunately, in the case of the development of ARCS this important component of the instrument was addressed by inclusion in the Caltech grant funds to develop software for data reduction and analysis. The resulting package, known as DRCS or DrChops,[27] provided critical support for the commissioning of ARCS and has also been a model for further software development. Some portions of the software are a translation into C++ of data reduction routines written for the Pharos instrument at Los Alamos National Laboratory. The library of routines in DrChops may be called from PYTHON, a modern object-oriented high-level language. With judicious choices for the roles of C++ and PYTHON, DrChops uses the flexibility of PYTHON for developing a user application while retaining nearly all of the computational speed of compiled C++ codes. Some reduction routines are written to run in parallel on multiprocessor computing clusters, yielding a factor of 10 improvement in reduction speed when using 12 cores compared to one.

The software for data reduction and analysis is based on four concepts: instrument, measurement, histogram, and reduction operators. An instrument is a hierarchy of components, a powerful construct that is also used in the recently developed MCViNE Monte Carlo neutron scattering simulation software.[42] A measurement maintains a reference to the instrument and consists of one or more experimental runs. Each experimental run is a container of histogrammed data and meta-data about the run. A histogram is the fundamental data object, used to represent all measured and reduced data. Reduction operators work on measurements and histograms to perform operations such as binning, rebinning, background correction, and normalizations. Due to the object-oriented design and the modularity of the software, it is possible to accommodate substantial changes to the routines quickly. In the commissioning phase of ARCS, for example, it was possible to modify reduction routines quickly and provide diagnostic tools for ARCS as PYTHON scripts adapted for data stored in the SNS event mode.

Interaction with the data reduction and analysis software may be tailored to the experience and needs of the user. For typical use, a command line script is run which takes text files as input to do data reduction to standard formats in a batch mode. A graphical user interface, known as HistogramGUI, is available as well, providing visualization of the intermediate stages of reduction if desired. More experienced users that want to manipulate the data directly may download the source code and instructions for working within the framework provided by DrChops. Development of new reduction techniques is done in PYTHON, which allows rapid exploration of new features. For example, multiple scattering corrections for phonon density-of-states measurements may be automated and methods of analyzing sweep mode data may

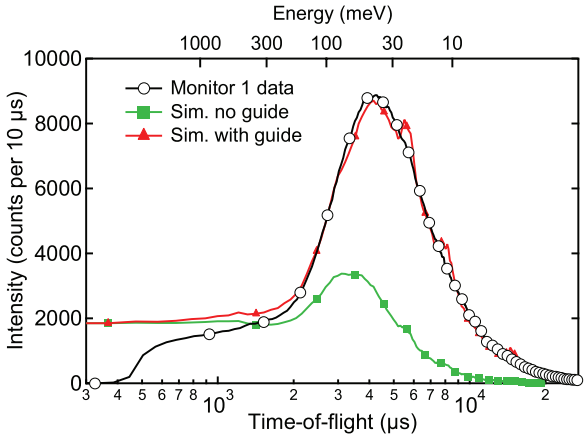

FIG. 5. (Color online) ARCS beam monitor data compared to absolute intensity Monte Carlo calculations with and without the ARCS neutron guide. Symbols are shown for every 50 data points. The data from the monitor below ~1 ms are not reliable due to the high prompt pulse radiation.

be rapidly explored. The ARCS software effort has provided a valuable tool for chopper spectrometer data reduction and analysis and has given the community a model of software development for new neutron scattering instrumentation.

III. INSTRUMENT PERFORMANCE

There are a number of ways to judge the performance of an instrument. Comparing neutron data, both from beam monitors as well as scattering from known samples, to analytical and simulated results provides confirmation that the components of the system are working properly and in a predictable manner. It is also useful to assess scientific measurements from the instrument for feedback on the overall instrument operations and suggestions for improvements to enable new science. This section explores both types of performance of ARCS.

A. Intensity and resolution measurements

With no choppers in place, the signal in the first beam monitor allows the source and guide performance to be characterized. Figure 5 shows counts per 10 μs time bins in the upstream ARCS beam monitor ($L_{m1} = 11.83$ m) during a measurement of ~800 s at an SNS beam power of 125 kW operating at 30 Hz. The monitor was calibrated by the SNS detector group and found to have an efficiency of $(1.0 \pm 0.1) \times 10^{-5}$ at a wavelength of 1.8 Å. This monitor uses a low pressure of ^{3}He gas, and thus has an efficiency proportional to wavelength. The ARCS monitor does not provide reliable data at times less than ~1 ms after the proton pulse on target due to the high level of prompt radiation. The peak at moderate neutron energies is clearly seen in the data, corresponding to the partially thermalized beam from the 25 mm depth poisoned, decoupled water moderator.

Also plotted in Fig. 5 are the absolute intensities expected from the calibrated beam monitor based on a Monte Carlo (MC) simulation of ARCS using the MCViNE software package.[41] The source term was the 25 mm poison-depth water SNS moderator component distributed with the McStas MC program,[43] which uses tabulated calculations of the expected moderator output based on detailed simulations of the SNS source.[35] Calculations with and without the neutron guide before the monitor position are shown. The guide gain is a factor of two for 140 meV neutrons, and rises to a factor of ten for 12 meV based on the simulations. When scaled by the appropriate integrated power of the measurement and the energy-dependent monitor efficiency, the simulation and moderator data sets agree within reasonable accuracy, demonstrating that the instrument source and guide perform as expected.

The performance of the ARCS Fermi choppers and the instrumental resolution was tested by scattering from vanadium and the sharp excitations from a small molecule. Figure 6 shows the scattering of a 100 meV monochromatic beam from a 6.4 mm diameter, 5 cm tall vanadium rod into the middle detector row ($L_3 = 3.0$ m) versus the neutron time-of-flight (Fig. 6(b)), along with data from monitor 1 (Fig. 6(a)) and the downstream monitor 2 ($L_{m2} = 18.5$ m, Fig. 6(c)). These data are compared to the MC simulation of the beam monitors and an ideal isotropic elastic scatterer. The results have been scaled by factors of 1.8, 2.3, and 1.6 for Figs. 6(a)–6(c), respectively, so that the peak of each experimental data set matches the simulation. This scaling represents uncertainty in the transmission through material not in the simulation, e.g., aluminum vacuum windows, the aluminum spacers between absorbing blades of the Fermi chopper and air gaps in the neutron flight path, as well as possible errors in the efficiency of the neutron detectors as simulated. This aspect of the model continues to be investigated. Given this scaling, the data demonstrate the good agreement between the measured and simulated peak widths. A logarithmic plot of the monitor 2 intensity (Fig. 6(c) inset) shows that the simulation and data agree in the fall off of the tails of the source distribution as well.

It is useful to have a simple method to predict the instrumental resolution as an aid in planning experiments, and a tool for comparing sample calculations to real data with little additional computational overhead. By considering the contributions to the timing uncertainty from the source, chopper opening and path length differences to be statistically independent and added in quadrature, an analytical function for the resolution of a chopper spectrometer can be written as

$$\frac{d\omega}{E_i} = 2\sqrt{\left(1+\frac{L_2}{L_3}\left(\frac{v_f}{v_i}\right)^3\right)^2\left(\frac{dt_m}{t_1}\right)^2 + \left(1+\frac{L_1+L_2}{L_3}\left(\frac{v_f}{v_i}\right)^3\right)^2\left(\frac{dt_c}{t_1}\right)^2 + \left(\frac{v_f}{v_i}\right)^4\left(\frac{dL_3}{L_3}\right)^2}, \quad (1)$$

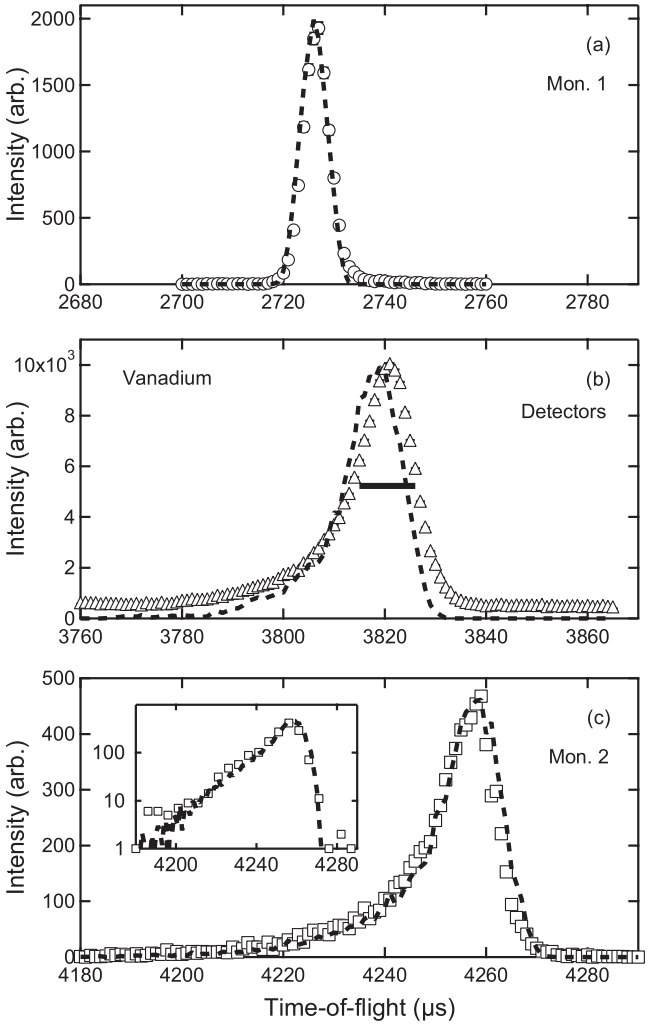

FIG. 6. ARCS monitor and vanadium scattering data (symbols) compared to simulation (dashed lines). All data correspond to measurements with a 6.4 mm diameter 5 cm tall vanadium rod with an incident energy of 100 meV. The time-of-flight spectra are measured/calculated at the (a) first beam monitor, (b) the middle detector row, and (c) the second or downstream beam monitor. The inset in (c) is the same data shown in panel (c) on a logarithmic intensity scale.

where E_i is the incident energy, t_1 is the neutron time-of-flight to the chopper, v_i and v_f are the initial and final neutron velocities, respectively, dt_m is the time spread of the moderator, dt_c is the time pulse width through the Fermi chopper, and dL_3 is a path length uncertainty representing the sample and detector sizes.[2] For the purposes of modeling the ARCS resolution with this simple expression, we take the first beam monitor's full-width-at-half-maximum (FWHM) to be the chopper timing uncertainty dt_c and use the FWHM of the tabulated pulse shape at E_i from the SNS moderator simulation as dt_m.[35] The path length variation dL_3 is less well defined and is taken as something approximately equal to a typical sample dimension or detector penetration depth. The horizontal bar in Fig. 6(b) represents the value found from Eq. (1) converted to time-of-flight using $dL_3 = 2.5$ cm and the appropriate chopper (monitor 1) and moderator widths and compares well with both the measured and simulated FWHM.

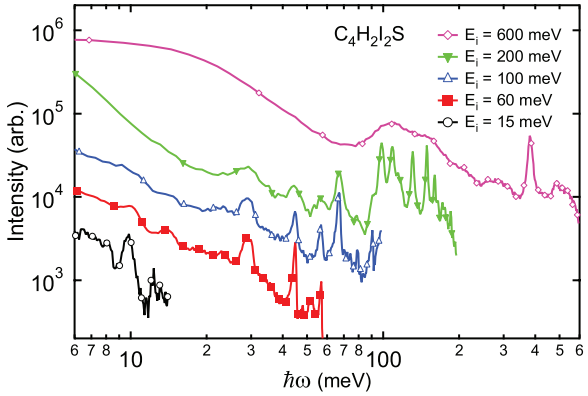

FIG. 7. (Color online) Inelastic scattering spectra for 2,5-diiodothiophene ($C_4H_2I_2S$) versus incident energy. Data were acquired at several incident energies, and are offset vertically for presentation. Symbols are shown for every 10 datapoints. Details of chopper configurations are described in the text.

The energy transfer dependence of the resolution function can be determined using a sample with sharp excitations. The compound 2,5-diiodothiophene ($C_4H_2I_2S$) has many rotational and vibrational energy modes spread from a few to hundreds of meV and has been used previously to characterize the energy resolution of neutron spectrometers.[24,44] Figure 7 shows the inelastic scattering from $C_4H_2I_2S$ for various chopper settings on ARCS, integrated over the scattering angle from 3° to 30°. The powder sample was loaded in an aluminum flat plate holder with dimensions 5cm × 5cm × 0.2cm and cooled to 50 K, oriented at 45° with respect to the incident beam to avoid self-shadowing of the detectors. The spectra measured at several incident energies are offset vertically in the figure for clarity. ARCS Fermi chopper 1 (slat spacing $d = 1.5$ mm, curvature $r = 1.4$ m) was used with an incident energy of 600 meV at 600 Hz. Fermi chopper 2 ($d = 1.5$ mm, $r = 0.58$ m) was set for 15 meV (240 Hz), 60 meV (480 Hz), 100 meV (600 Hz), and 200 meV (600 Hz). The data represent almost two decades of energy transfer range that can be measured on ARCS.

To quantify the dependence of the energy resolution on energy transfer, peaks in the spectra shown in Fig. 7 were fit to a Gaussian lineshape with a sloping background. The FWHM of the resulting fits are plotted in Fig. 8, with the error bars determined by the statistical uncertainty of the fits. For the elastic width, the Gaussian shape did not give a good representation due to the asymmetric moderator contribution, so a numerical determination of the FWHM was used. Some of the peaks have additional widths beyond the instrument resolution, such as the peak near 30meV, but the majority provides a reasonable measure of the ARCS resolution for different chopper settings. The solid lines are the calculated FWHM using Eq. (1) to determine the expected value based on the monitor 1 width (dt_c) from each measurement, the SNS moderator width (dt_m) and a path length uncertainty dL_3 of 2.5 cm was used for all cases. At the elastic position, the calculated values are all within 10% of the measurement. For larger energy transfers, however, the simple model for the resolution seems to underestimate the Gaussian fit results.

To further explore the energy resolution as a function of energy transfer for ARCS, simulations were made of an ideal

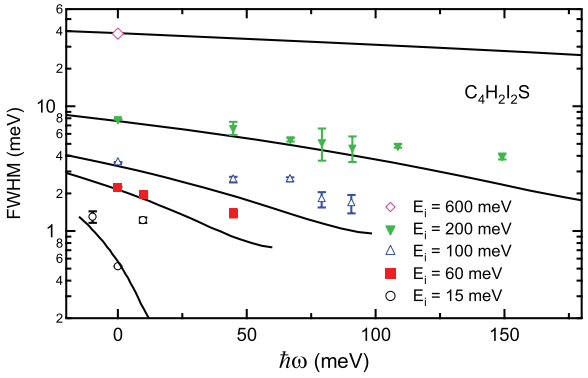

FIG. 8. (Color online) Measured FWHM of excitations in 2,5-diiodothiophene ($C_4H_2I_2S$) for different incident energies. Solid lines are calculations of the resolution function as described in the text. The peak near 30meV seen in Figure 7 is not used for comparison due to intrinsic broadening.

inelastic scatterer with the shape of the $C_4H_2I_2S$ sample for $E_i = 100$ meV using MCViNE. Figure 9 shows the measured spectrum compared to the simulation for energy transfers of 0, 29.5, 45.1, 56.6, 67.4, 79.5, and 91.0 meV, where the simulated data have been scaled to the measured peak intensities. A Lorenzian plus second order polynomial background have been added to the MC calculations to account for instrument background and multiphonon processes. Note that the asymmetry of the lineshape due to the moderator pulse shape is an important feature of the simulation and measurement for ARCS in this energy range. The simulation provides an excellent representation of the data for the elastic scattering as well as most of the selected inelastic peaks. It is evident that the measured peak near 30 meV includes additional broadening or other peaks that ARCS cannot resolve for these instrument settings. These results indicate why the Gaussian fits used to extract the peak widths for Fig. 8 were larger than the estimated resolution, since the symmetric function could not capture the tail of the resolution due to the moderator pulse shape. It is important to have simple analytical models of the instrument performance, but these results emphasize the need

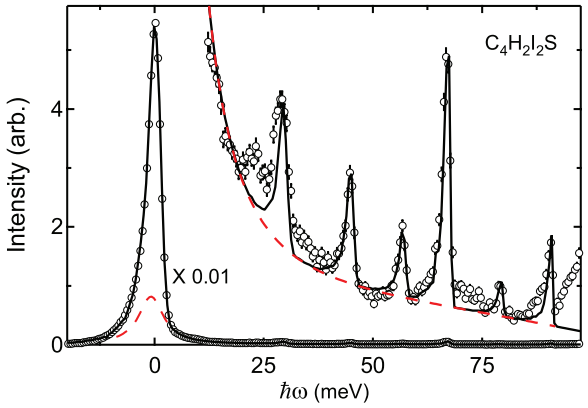

FIG. 9. (Color online) Inelastic scattering spectrum for 2,5-diiodothiophene ($C_4H_2I_2S$) for $E_i = 100$ meV measured on ARCS. Data (open circles) are compared to a MC instrument simulation (solid line) of an ideal scatterer with the same dimensions and orientation as the sample, as described in the text. A Lorenzian plus second order polynomial background (dashed line) is shown.

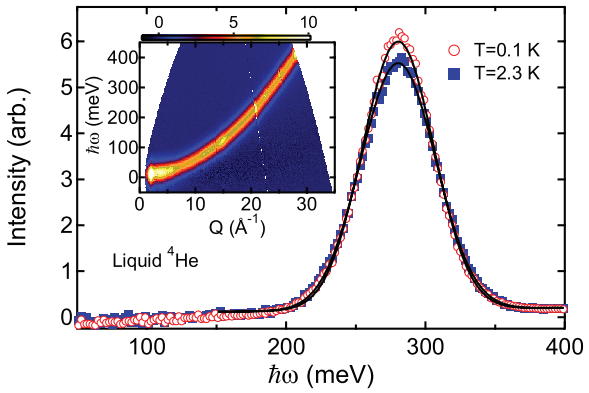

FIG. 10. (Color online) Inelastic scattering from liquid ^{4}He. Data correspond to constant wave vector cuts through the helium recoil line integrated between $23 < Q < 23.5$ inverse Angstroms. Inset shows the measured scattering intensity as a function of energy and wave vector transfer. An empty cell measurement was used as a measure of the background and subtracted from these data. Measurements are further described in the text. Solid lines correspond to simple Gaussian fits.

for continued efforts to provide more sophisticated modeling and analysis software for chopper spectrometers to accurately correct for instrumental resolution effects.

B. Scientific examples

We provide here two scientific examples which make use of the large angular coverage of the ARCS instrument and its large range of incident neutron wavelengths. Inelastic neutron scattering measurements of liquid helium have been a staple of neutron spectrometers for decades. A proof-of-principle measurement was performed on liquid ^{4}He to investigate the suitability of using ARCS for further studies of such systems. We also describe a single crystal phonon measurement of the semiconductor FeSi. These data illustrate the ability to measure many Brillouin zones simultaneously with short measurement times using ARCS.

For the liquid ^{4}He measurements, a large cylindrical aluminum sample cell (~100 cc) that can be pressurized to 100 bars was constructed by the sample environment team at SNS. Such a large volume is desirable in view of the relatively low ^{4}He scattering cross section. A cryostat large enough to accommodate the cell that has a base temperature (without sample) of 30 mK was also commissioned. Liquid ^{4}He was measured at $T = 0.1$ and 2.3 K with an incident energy of 700 meV using the ARCS instrument. The $T = 2.3$ K spectrum is shown as an inset to Fig. 10. The helium recoil line is clearly evident at large energy and wave vector transfers. The width of this recoil line is directly related to the mean kinetic energy of atoms. The onset of the superfluid state can be inferred from a drop in the kinetic energy (or a narrowing of the width) at low temperatures when some of the atoms enter the condensate.[6] Figure 10 shows constant wave vector cuts through the recoil spectrum at $T = 0.1$ and 2.3 K. There is clearly a notable change in absolute intensity as the temperature is reduced. Investigations of the Bose-Einstein Condensate and the elementary excitations in ^{4}He and ^{3}He-^{4}He mixtures are also being planned.[45]

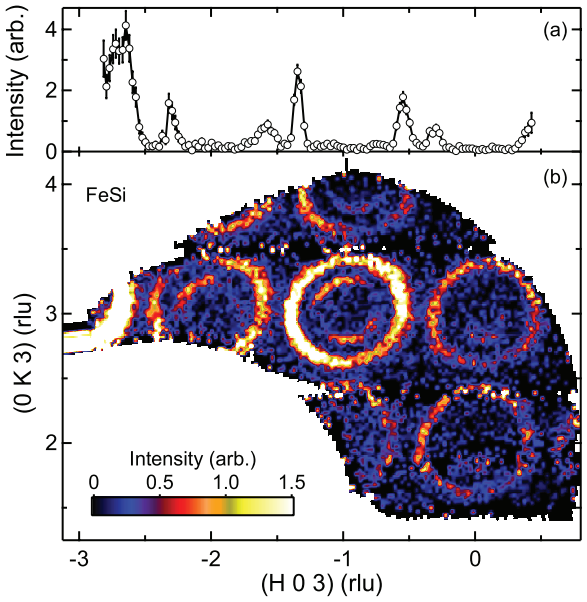

FIG. 11. (Color online) Inelastic neutron scattering spectra examining the phonon scattering for a single crystal of FeSi. Details of the measurement are described in the text. Panel (b) corresponds to integrating data between 15 and 17 meV and plotting the result in the (HK3) plane for L = 3 ± 0.1. Panel (a) corresponds to a cut through the data in (b) for K = 3 ± 0.1 and L = 3 ± 0.1.

FeSi has been categorized as a narrow-gap semiconductor[46] and is also of interest as a candidate thermoelectric material.[47] To further characterize this system, a study of the temperature dependent phonon scattering for powders and single crystals has been performed using ARCS. The FeSi single crystal measurements were performed with an incident energy of 40 meV at $T = 10$ K. The 8.5 g sample was mounted with the (HHL) plane horizontal, and thirty individual rotations about the vertical axis were measured in 1° steps. Each measurement accumulated data for ∼20 min with the neutron source operating at a beam power of 850 kW. A projection of the scattering intensity in the (HK3) plane for energy transfer integrated between 15 and 17 meV is shown in Fig. 11(b). The rings correspond to acoustic phonons propagating outward from the nuclear Bragg peak positions. Note that the intensity variations around the rings follow the $\mathbf{Q}\cdot\boldsymbol{\varepsilon}$ dependence for wave vector transfer $\mathbf{Q}$ and polarization vector $\boldsymbol{\varepsilon}$ relative to the nearby Brillioun zone center. As expected, the inner circle of scattering is a longitudinal acoustic phonon (steeper dispersion) while the outer ring is from the transverse acoustic phonons. Figure 11(a) illustrates a single cut through the data in panel (b) along the (H33) axis, analogous to a triple-axis constant E scan. The temperature dependent behavior of the phonon modes can be correlated to temperature dependent changes in the physical properties of the compound to help discover the underlying physical mechanisms for those changes.

IV. FUTURE DIRECTIONS FOR ARCS

Continual upgrades and maintenance are a natural part of the life-cycle of scientific instruments at a user facility. ARCS has upgraded portions of the instrument since the time of entering the user program. For example, a transmission neutron camera has been developed for use in the sample vacuum chamber. This device makes use of a commercially available neutron camera. The camera drops in behind the sample position and is used for verifying the heights and location of samples relative to the beam position. The camera also allows one to visualize the positions of horizontal and vertical apertures for both powder and single crystal samples.

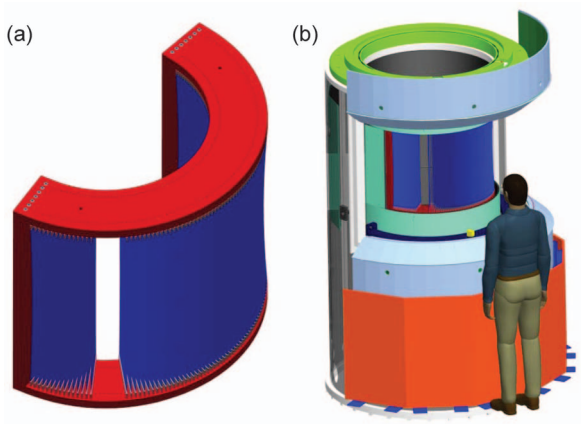

FIG. 12. (Color online) ARCS radial collimator renderings. (a) Oblique view of radial collimator from above the beam position. Absorbing foils are not being installed in the vicinity of the through beam to avoid any additional scattering by the direct beam. (b) Installed view of radial collimator as viewed from within the detector chamber. Individual is shown for scale. Material around the sample and detector chamber interface is boron carbide based neutron shielding.

A medium resolution radial collimator is currently being developed to be placed in the scattered beam. A rendering of the radial collimator as designed is shown in Fig. 12(a), and Fig. 12(b) is a rendering of the collimator in the installed position. The collimator was designed to limit the scattering seen by the detectors to the region just around the sample position, thereby eliminating background from heat shields, vacuum shrouds, or other parts of complex sample environments. The collimator has an inner radius of 0.3 m, an outer radius of 0.47 m, and an angular blade separation of 1.6°. There are no supporting posts for the collimator within the range of scattering angles of the instrument, and the collimator blades and the aluminum structure are coated with ^{10}B enriched boron carbide as a neutron absorber. A support mechanism is being designed to allow the collimator to oscillate in the scattering plane about the sample axis, and to allow the entire collimator assembly to move vertically downward out of the scattered beam position when not in use.

There are several future upgrades being considered and developed for ARCS. One of these is the availability of low-background sample environments tailored for the large scattering angle of the instrument. This often entails making thin windows and shielding other portions of heat shields of furnaces or cryostats. Other sample environment upgrades specific to ARCS being pursued are motorized sample goniometer tilts for single crystals and gas pressure cells for *in situ* measurements. Another upgrade path includes installing a second T_0 chopper. As noted above, there is currently room available for this chopper, and it would allow for additional

control of the transmitted neutron beam and provide background reduction. Further Fermi chopper development is also being pursued. Additional chopper packages are being designed to take advantage of the large range of thermal and epithermal neutrons available, while also considering the initial instrument users configuration choices and experimental boundary conditions. Experience is being gained at the SNS in polarization analysis for time-of-flight instrumentation, e.g., at the Magnetism Reflectometer (beamline 4A) using supermirrors. Filter polarization techniques are being developed for the HYSPEC spectrometer (beamline 14B). There is potential for polarizing the incident and a portion of the scattered beam at ARCS. Maintenance of guide fields and ^{3}He polarization cells in the high vacuum environment of ARCS are clear obstacles which will require significant development to overcome.

V. CONCLUSION

ARCS is a fully commissioned, versatile Fermi chopper spectrometer in the neutron sciences user program of the Spallation Neutron Source at the Oak Ridge National Laboratory. Based upon a series of measurements examining a wide range of samples and physics, the instrument is performing very well. As the SNS facility increases its power to the target, more experiments will be possible using smaller samples and less measurement time, providing even more scientific productivity for the neutron scattering community.

ACKNOWLEDGMENTS

The ARCS project was only made possible by the support of numerous colleagues at the SNS, Caltech and the IDT members. In particular, expert design work was provided by K. Shaw and S. Howard, outstanding support for neutronic calculations by E. Iverson, and excellent project management by P. Albertson and B. Thibadeau. Many essential discussions were held with J. Ankner, J. Carpenter, G. Ehlers, G. Granroth, M. Hagen, and K. Herwig. We acknowledge T. Kelley for his work on creating the early version of the reduction software, and M. Aivazis for his guidance on software architecture and design. We thank D. Mikkelson, R. Mikkelson, and A. Schultz for developing the ISAW handling of ARCS data. A. Kolesnikov graciously provided the idea and sample for the $C_4H_2I_2S$ measurement. Data for the liquid ^{4}He measurement were provided by S. Diallo, R. Azuah and H. Glyde. Data for the FeSi single crystal measurements were provided by O. Delaire. ARCS was supported by the DOE under Grant No. DE-FG02-01ER45950. ORNL/SNS is managed by UT-Battelle, LLC, for the DOE under Contract No. DE-AC05-00OR22725. Research at the SNS was sponsored by the Scientific User Facilities Division, Office of Basic Energy Sciences, DOE.

[1]E. Fermi, J. Marshall, and L. Marshall, Phys. Rev. **72**, 193 (1947).
[2]C. G. Windsor, *Pulsed Neutron Scattering* (Taylor & Frances, London, 1981).
[3]G. Balakrishnan, N. R. Bernhoeft, Z. A. Bowden, D. McK. Paul, and A. D. Taylor, Nature (London) **327**, 45 (1987).
[4]D. L. Price and J. M. Carpenter, J. Non-Cryst. Solids **92**, 153 (1987).
[5]S. Kern, C.-K. Loong, and G. H. Lander, Phys. Rev. B **32**, 3051 (1985).
[6]H. R. Glyde, R. T. Azuah, and W. G. Stirling, Phys. Rev. B **62**, 14337 (2000).
[7]D. A. Tennant, T. G. Perring, R. A. Cowley, and S. E. Nagler, Phys. Rev. Lett. **70**, 4003 (1993).
[8]T. E. Mason, D. Abernathy, I. Anderson, J. Ankner, T. Egami, G. Ehlers, A. Ekkebus, G. Granroth, M. Hagen, K. Herwig, J. Hodges, C. Hoffmann, C. Horak, L. Horton, F. Klose, J. Larese, A. Mesecar, D. Myles, J. Neuefeind, M. Ohl, C. Tulk, X.-L. Wang, and J. Zhao, Physica B **385–386**, 955 (2006).
[9]D. L. Price, J. M. Carpenter, C. A. Pelizzari, S. K. Sinha, I. Bresof, and G. E. Ostrowski, *Proceedings of the 6th Meeting of the International Collaboration on Advanced Neutron Sources (ICANS VI), 1982*, Argonne National Laboratory, Argonne, Illinois, USA, Report ANL-82-80 (1983), p. 207.
[10]S. Itoh, M. Arai, and M. Kawai, *Proceedings of the 15th Meeting of the International Collaboration on Advanced Neutron Sources (ICANS XV), 2000*, High Energy Accelerator Research Organization (KEK), Ibaraki-ken, Japan, Report KEK 2000-22 (2001), p. 425.
[11]A. D. Taylor, B. C. Boland, and Z. A. Bowden, *Proceedings of the 9th Meeting of the International Collaboration on Advanced Neutron Sources (ICANS IX), 1987*, edited by F. Atchison and W. Fischer (Swiss Institute for Nuclear Research, Villigen, Switzerland, 1987), p. 349; A. D. Taylor, M. Arai, S. M. Bennington, Z. A. Bowden, R. Osborn, K. Anderson, W. G. Stirling, T. Nakane, K. Yamada, and D. Welz, *Proceeding of the 11th Meeting of the International Collaboration on Advanced Neutron Sources (ICANS XI), 1990*, edited by M. Misawa, M. Furusaka, H. Ikeda, and N. Watanabe, National Laboratory for High Energy Physics (KEK), Ibaraki-ken, Japan, Report 90-025 (1991), p. 705.
[12]R. A. Robinson, M. Nutter, R. N. Silver, D. T. Hooten, and R. L. Rickets, *Proceedings of the 10th Meeting of the International Collaboration on Advanced Neutron Sources (ICANS X), 1988*, Institute of Physics Conference Series Vol. 97, edited by D. K. Hyer (Institute of Physics, Bristol, England, 1989), p. 403; R. J. McQueeney and R. A. Robinson, Neutron News **14**, 36 (2003).
[13]T. G. Perring, A. D. Taylor, R. Osborn, D. McK. Paul, A. T. Boothroyd, and G. Aeppli, *Proceedings of the 12th Meeting of the International Collaboration on Advanced Neutron Sources (ICANS XII), 1993*, Rutherford Appleton Laboratory, Didcot, UK, RAL Report 94-025 (1994), p. I-60.
[14]C. D. Frost and T. G. Perring, *Proceedings of the 15th Meeting of the International Collaboration on Advanced Neutron Sources (ICANS XV), 2000*, High Energy Accelerator Research Organization (KEK), Ibaraki-ken, Japan, Report KEK 2000-22 (2001), p. 405.
[15]R. I. Bewley, R. S. Eccleston, K. A. McEwen, S. M. Hayden, M. T. Dove, S. M. Bennington, J. R. Treadgold, and R. L. S. Coleman, Physica B **385–386**, 1029 (2006); R. I. Bewley, T. Guidi, and S. M. Bennington, "MERLIN: a high count rate chopper spectrometer at ISIS," Notiziario Neutroni e Luce di Sincrotrone **14**(1), 22–27 (2009).
[16]R. Kajimoto, T. Yokoo, K. Nakajima, M. Nakamura, K. Soyama, T. Ino, S. Shamoto, M. Fujita, K. Ohoyama, H. Hiraka, K. Yamada, and M. Arai, J. Neutron Res. **15**, 5 (2007); S. Itoh, T. Yokoo, S. Sato, S. Yano, D. Kawana, J. Suzuki, and T. Sato, Nucl. Instrum. Methods Phys. Res. A **631**, 90 (2011).
[17]G. E. Granroth, D. H. Vandergriff, and S. E. Nagler, Physica B **385–386**, 1104 (2006).
[18]D. L. Abernathy, "ARCS: a wide Angular-Range Chopper Spectrometer at the SNS," Notiziario Neutroni e Luce di Sinctrotrone **13**(1), 4–7 (2008).
[19]D. L. Abernathy, in *Proceedings of the International Conference on Neutron Scattering, Munich, Germany, (2001);* Appl. Phys. A **74** (Suppl.), S1595–S1597 (2002).
[20]G. Granroth, D. Abernathy, G. Ehlers, M. Hagen, K. Herwig, E. Mamontov, M. Ohl, and C. Wildgruber, *Proceedings of the 18th Meeting of the International Collaboration on Advanced Neutron Sources (ICANS XVIII), 2007*, edited by J. Wei, S. Wang, W. Huang and J. Zhao, (Institute of High Energy Physics, Beijing, China, 2007), p. 350.
[21]M. Ohl, M. Monkenbush, and D. Richter, Physica B **355**, 153 (2003).
[22]E. Mamontov and K. W. Herwig, Rev. Sci. Instrum. **82**, 085109 (2011).
[23]G. Ehlers, A. A. Podlesnyak, J. L. Niedziela, E. B. Iverson, and P. E. Sokol, Rev. Sci. Instrum. **82**, 085108 (2011).
[24]G. E. Granroth, A. I. Kolesnikov, T. E. Sherline, J. P. Clancy, K. A. Ross, J. P. C. Ruff, B. D. Gaulin, and S. E. Nagler, in *Proceedings of the International Conference on Neutron Scattering, Knoxville, TN, USA, 2009* [J. Phys.: Conf. Ser. **251**, 012058 (2010)].
[25]S. M. Shapiro, I. A. Zaliznyak, L. Passel, V. J. Ghosh, W. J. Leonhard, and M. E. Hagen, Physica B **385–386**, 1107 (2006).
[26]See http://neutrons.ornl.gov/instruments for information about the entire

instrument suite at the ORNL neutron scattering sources SNS and HFIR.
[27]See http://docs.danse.us/DrChops for documentation and software download. Further software developments have been made under a new software initiative called DANSE, see http://danse.us.
[28]A. D. Christianson, M. D. Lumsden, O. Delaire, M. B. Stone, D. L. Abernathy, M. A. McGuire, A. S. Sefat, R. Jin, B. C. Sales, D. Mandrus, E. D. Mun, P. C. Canfield, J. Y. Y. Lin, M. Lucas, M. Kresch, J. B. Keith, B. Fultz, E. A. Goremychkin, and R. J. McQueeney, Phys. Rev. Lett. **101**, 157004 (2008).
[29]D. Parshall, K. A. Lokshin, J. Niedziela, A. D. Christianson, M. D. Lumsden, H. A. Mook, S. E. Nagler, M. A. McGuire, M. B. Stone, D. L. Abernathy, A. S. Sefat, B. C. Sales, D. G. Mandrus, and T. Egami, Phys. Rev. B **80**, 012502 (2009).
[30]M. D. Lumsden, A. D. Christianson, D. Parshall, M. B. Stone, S. E. Nagler, H. A. Mook, K. Lokshin, T. Egami, D. L. Abernathy, E. A. Goremychkin, R. Osborn, M. A. McGuire, A. S. Sefat, R. Jin, B. C. Sales, and D. Mandrus, Phys. Rev. Lett. **102**, 107005 (2009).
[31]M. D. Lumsden, A. D. Christianson, E. A. Goremychkin, S. E. Nagler, H. A. Mook, M. B. Stone, D. L. Abernathy, T. Guidi, G. J. MacDougall, C. de la Cruz, A. S. Sefat, M. A. McGuire, B. C. Sales, and D. Mandrus, Nat. Phys. **6**, 182 (2010).
[32]O. Delaire, A. F. May, M. A. McGuire, W. D. Porter, M. S. Lucas, M. B. Stone, D. L. Abernathy, and G. J. Snyder, Phys. Rev. B **80**, 184302 (2009).
[33]M. S. Lucas, J. A. Muñoz, L. Mauger, Chen W. Li, A. O. Sheets, Z. Turgut, J. Horwath, D. L. Abernathy, M. B. Stone, O. Delaire, Yuming Xiao, and B. Fultz, J. Appl. Phys. **108**, 023519 (2010); M. S. Lucas, J. A. Muñoz, O. Delaire, N. D. Markovskiy, M. B. Stone, D. L. Abernathy, I. Halevy, L. Mauger, J. B. Keith, M. L. Winterrose, Yuming Xiao, M. Lerche, and B. Fultz, Phys. Rev. B **82**, 144306 (2010); J. A. Muñoz, M. S. Lucas, O. Delaire, M. L. Winterrose, L. Mauger, Chen W. Li, A. O. Sheets, M. B. Stone, D. L. Abernathy, Yuming Xiao, Paul Chow, and B. Fultz, Phys. Rev. Lett. **107**, 115501 (2011).
[34]E. S. Bozin, P. Juhas, W. Zhou, M. B. Stone, D. L. Abernathy, A. Huq, and S. J. L. Billinge, J. Appl. Crystallogr. **42**, 724 (2009).
[35]E. B. Iverson, P. D. Ferguson, F. X. Gallmeier, and I. I. Popova, Technical Report SNS 110040300-DA0001-R00, 2002.
[36]See http://www.skf.com/portal/skf_rev/home for SKF Magnetic Bearings, Calgary, Canada.
[37]T. G. Worlton, A. Chatterjee, J. P. Hammonds, C. Bouzek, D. J. Mikkelson, R. Mikkelson, M. Miller, B. Serum, and P. F. Peterson, Neutron News **15**(3), 14 (2004). For documentation and software download, see http://ftp.sns.gov/ISAW/.
[38]See http://mslice.isis.rl.ac.uk/Main_Page for the data visualization software Mslice developed by R. Coldea in Matlab and Fortran; see http://www.ncnr.nist.gov/dave/ for an adaption based on IDL.
[39]R. A. Riedel, R. G. Cooper, L. L. Funk, and L. G. Clonts, Nucl. Instrum. Methods A **664**, 366–369 (2012).
[40]See http://www.dielectricsciences.com for information about ZHIP mix, developed in collaboration with Dielectric Sciences, Inc.
[41]H. Nojiri, S. Yoshii, M. Yasui, K. Okada, M. Matsuda, J.-S. Jung, T. Kimura, L. Santodonato, G. E. Granroth, K. A. Ross, J. P. Carlo, and B. D. Gaulin, Phys. Rev. Lett. **106**, 237202 (2011).
[42]See http://docs.danse.us/MCViNE for documentation and software download.
[43]K. Lefmann and K. Nielsen, Neutron News **10**, 20 (1999).
[44]P. C. H. Michell, presented at the *18th North American Catalysis Society Meeting, Cancun, Mexico, 2003*, see http://www.nacatsoc.org/18nam/Orals/168-Mitchell-Hydrogen%20in%20Hydrotreating%20and%20Other%20Catalysts.pdf.
[45]S. O. Diallo, J. V. Pearce, R. T. Azuah, O. Kirichek, J. W. Taylor, and H. R. Glyde, Phys. Rev. Lett. **98**, 205301 (2007).
[46]Z. Schlesigner, Z. Fisk, H.-T. Zhang, M. B. Maple, J. DiTusa, and G. Aeppli, Phys. Rev. Lett. **71**, 1748 (1993).
[47]B. C. Sales, E. C. Jones, B. C. Chakoumakos, J. A. Fernandez-Baca, H. E. Harmon, J. W. Sharp, and E. H. Volckmann, Phys. Rev. B **50**, 8207 (1994).